自动焊接相贯线接缝的实时插补控制算法与仿真

霍孟友， 王新刚， 尹 萍
（山东大学 机械工程学院，济南 250061）

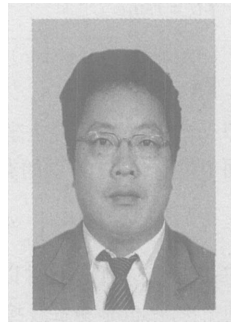

霍孟友

摘 要：圆柱管之间连通焊接是较为广泛的管连接形式之一，而形成的相贯线接缝则是较为复杂的空间曲线。在一种专用焊接机床的基础上，以圆柱管之间连通焊接形式为例，介绍了实现复杂相贯线接缝自动焊接的可控步长实时插补控制算法，重点研究了保持焊接速度恒定以及满足给定逼近误差条件时利用等长直线段拟合复杂空间曲线的插补计算处理方法。以一种通用的圆柱管之间连通焊接应用为例进行了实时控制算法计算说明，并且利用OpenGL工具软件对插补合成运动轨迹进行了动态仿真。仿真结果表明，该实时插补控制算法是可行的。

关键词：相贯线接缝；焊接；插补算法；仿真；OpenGL工具软件
中图分类号：TP391 文献标识码：A 文章编号：0253－360X(2006)11－037－04

0 序 言

在生产实际中，圆柱管之间的连通焊接是较为广泛的管连接形式之一，所形成的接缝则是较为复杂的相贯线。因此，如何控制焊枪或工件的运动，使机床焊接出满足精度要求的焊缝轨迹，就成为自动化焊接机床首先应该解决的问题，也是机床自动化控制的核心问题。文中基于一种专用焊接机床，研究了实现自动焊接圆柱管之间复杂相贯线接缝的实时插补控制算法，与文献[1]中提出的以时间 t 为变量的空间曲线可控步长插补方法相比，计算处理过程要简单许多，且插补时间固定，能很好的满足控制系统对实时性的要求，易于被机床的控制系统所实现。同时以圆柱管之间的一种通用连接形式为例，进行了插补计算处理，利用OpenGL工具软件对焊枪移动与焊接件回转合成的运行轨迹进行了动态仿真，并进一步对实时插补控制算法和数学模型进行修正与优化。通过仿真，证明了所研究的实时插补控制算法的可行性。

1 相交圆柱管相贯线接缝的数学模型

设相交两圆柱管的半径为 R 和 r，分别为主管和支管，且 $R>r$，两圆柱管轴线 Oy 和 OV 的交角为 α，如图1所示。焊接时工件绕轴旋转，焊枪沿相贯线移动。这里 α 角不宜小于30°，以保证施焊条件，使焊缝焊透[2]。

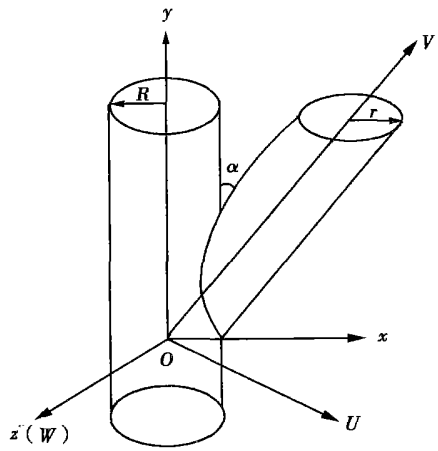

图1 相交双管示意图
Fig. 1 Schematic diagram of intersection pipe

在 $Oxyz$ 坐标系中，半径为 R 的圆柱管方程为

$$x^2+z^2=R^2。 \tag{1}$$

在 $OUVW$ 坐标系中，半径为 r 的圆柱管方程为

$$U^2+W^2=r^2。 \tag{2}$$

$OUVW$ 坐标系是将坐标系 $Oxyz$ 绕 Oz 轴顺时针旋转 α 角得到的，因此，两者之间的旋转变换关系为

$$\begin{bmatrix} x \\ y \\ z \end{bmatrix} = \begin{pmatrix} \cos\alpha & \sin\alpha & 0 \\ -\sin\alpha & \cos\alpha & 0 \\ 0 & 0 & 1 \end{pmatrix} \begin{bmatrix} U \\ V \\ W \end{bmatrix}。 \tag{3}$$

收稿日期：2005－10－18
基金项目：山东省自然科学基金资助项目(Y2004F16)

所以，半径为 R 的圆柱管方程在 $OUVW$ 坐标系中的描述则变为

$$(U\cos\alpha+V\sin\alpha)^2+W^2=R^2。\tag{4}$$

将式(2)与式(4)联立，就可得到半径分别为 R 与 r 的两个圆柱管相交所形成的焊接相贯线接缝在 $OUVW$ 坐标系中的参数方程为

$$\begin{cases}U=r\sin\varphi\\ V=(\sqrt{R^2-(r\cos\varphi)^2}-r\sin\varphi\cos\alpha)/\sin\alpha\\ W=r\cos\varphi\end{cases},\tag{5}$$

式中：φ 为相贯线接缝上坐标点(U, V, W)在 UOW 平面中投影点与 OW 轴的夹角，且

$$\varphi=\int_0^t\omega(t)\mathrm{d}t,\tag{6}$$

式中：$\omega(t)$是两个焊接件以 OV 作为回转轴同时回转的角速度，也是相贯线接缝绕 OV 轴旋转的瞬时角速度。由式(6)可以看出，控制焊接件以 $\omega(t)$角速度回转，同时控制焊枪使其沿着 OV 轴做轴向运动，该运动合成轨迹即是相贯线接缝。

2 可控步长实时插补控制算法

利用文中提及的专用焊接机床实现这种复杂空间曲线接缝的焊接，需要用空间直线段或圆弧去逼近被焊接曲线，该逼近过程即为插补。文中利用等长直线段逼近复杂空间曲线，即在保证给定逼近误差 ε 的前提下，用直线段 ΔL_i 代替圆弧 ΔS_i。$\Delta u(\varphi_i)$, $\Delta v(\varphi_i)$, $\Delta w(\varphi_i)$分别是 $\Delta L(\varphi_i)$在 OU, OV 和 OW 坐标轴上的位移分量，其中 $\Delta u(\varphi_i)$, $\Delta w(\varphi_i)$分别是焊接件在插补周期内回转角度后沿 OU 和 OW 轴产生的位移分量，$\Delta v(\varphi_i)$则是焊枪在插补周期内需要沿 OV 轴移动的位移量。在文中由于焊接件为圆柱，故焊枪在 OU、OW 轴上的位移分量均为零。这样插补的主要任务就变为：在恒插补周期 T 内，计算产生进给弦长 $\Delta L(\varphi_i)$所需要转过的角度 $\Delta\varphi_i$ 以及焊枪在 OV 坐标轴上移动的距离 $\Delta v(\varphi_i)$。利用 $\Delta\varphi_i$ 和 $\Delta v(\varphi_i)$作为控制量分别控制焊接件回转驱动电机和焊枪沿轴向运动控制步进电机，即可实现相贯线接缝的轨迹拟合。在恒定的插补周期内，利用变细分驱动技术控制步进电机可以完成给定量 $\Delta v(\varphi_i)$的移动控制。

这里插补步长 $\Delta L(\varphi_i)$由式(7)确定为

$$\Delta L(\varphi_i)=\{[U(\varphi_{i+1})-U(\varphi_i)]^2+[V(\varphi_{i+1})-V(\varphi_i)]^2+[W(\varphi_{i+1})-W(\varphi_i)]\}^{\frac{1}{2}}\quad(i=0,1,2,\ldots,n-1)。\tag{7}$$

设 s 为曲线弧长。利用空间曲线知识可知，描述式(5)的空间曲线弧长微分增量可以记为

$$\Delta s=\sqrt{(\frac{\mathrm{d}U}{\mathrm{d}\varphi})^2+(\frac{\mathrm{d}V}{\mathrm{d}\varphi})^2+(\frac{\mathrm{d}W}{\mathrm{d}\varphi})^2}。\tag{8}$$

进一步计算可得到

$$\frac{\mathrm{d}s}{\mathrm{d}\varphi}=r\sqrt{1+F^2},\tag{9}$$

式中：$F=\dfrac{r\sin\varphi\cos\varphi}{\sqrt{R^2+(r\cos\varphi)^2}}-\dfrac{\cos\varphi}{\tan\alpha}$。

为了获得稳定的焊接质量，进行实际焊接时应该维持焊接速度恒定，即单位时间内转过焊枪的弧线长度应该为一个固定常数。这里焊接速度设定为 v。插补步长 ΔL 与焊接速度 v 和插补周期 T 之间应满足如下关系

$$\Delta L=v\times T。\tag{10}$$

由于相贯线方程以 φ 为变量，而 φ 又是 t 的函数，所以有如下表达式

$$v=\frac{\mathrm{d}s}{\mathrm{d}t}=(\frac{\mathrm{d}s}{\mathrm{d}\varphi})\cdot(\frac{\mathrm{d}\varphi}{\mathrm{d}t})。\tag{11}$$

$$\frac{\mathrm{d}\varphi}{\mathrm{d}t}=\frac{v}{\mathrm{d}s/\mathrm{d}\varphi}=\frac{v}{r\sqrt{1+F^2}}。\tag{12}$$

根据数值求导公式，得

$$\varphi'(t_i)\approx\frac{\varphi(t_i+\Delta t)-\varphi(t_i)}{\Delta t}=\frac{\Delta\varphi_i}{T}\quad(i=0,1,2,\ldots,n-1)。\tag{13}$$

故有 $\Delta\varphi_i=vT/(r\sqrt{1+F^2})=\Delta L/r\sqrt{1+F^2}$。

(14)

将 $\Delta\varphi_i$ 代入 $\Delta\mathrm{L}(\varphi_i)$中，即可求得插补步长 $\Delta L(\varphi_i)$ 及其在各个坐标轴的分量。并且根据 $\Delta(\varphi_i)=\int_0^{t+\Delta t}\omega(t)\mathrm{d}t$ 就可得出焊接件的回转角速度，即

$$\omega(t)=\frac{\mathrm{d}\varphi}{\mathrm{d}t}=\frac{v}{r\sqrt{1+F^2}}。\tag{15}$$

利用长度为 ΔL(由式(10)决定)的空间直线段拟合相贯线焊缝时所产生的插补误差应小于等于给定的焊接逼近误差 ε，ε 约为 0.2～0.5 mm[3]。焊接速度 v 可根据焊接工艺要求选取一个符合工程实际的速度值，一般介于 5～50 mm/s 之间，而插补周期 T 也应该有一个合理的时间间隔，一般应≤25 ms (40 Hz)。如果插补周期太长，则运动过程不平稳，可能出现抖动，且插补误差增大。但是，因为受计算量的限制，插补周期也有最小时间限制，通常为几毫秒。

利用上面的插补算法可保证插补点始终在曲线上，没有累积误差，但存在弓高误差。弓高误差实际上就是插补误差。若对任意 $\varphi\in[0,2\pi]$，要求插补

步长 ΔL_i 逼近曲线弧 ΔS_i 所形成的弓高误差 ε_i 对所有插补点均有 $\varepsilon_i \leqslant \varepsilon$，根据给定的逼近误差 ε，可得最大插补步长为[1]

$$\Delta L_{max} = 2\sqrt{2R_f\varepsilon - \varepsilon^2}, \tag{16}$$

式中：R_f 是被插补圆弧的半径，它的大小由空间曲线的曲率 $k(\varphi)$和挠率 $r(\varphi)$决定，公式为

$$R_f = 1/\max[\max(k(\varphi)), \max(\tau(\varphi))]。 \tag{17}$$

为了满足给定的逼近误差，应该使得 $\Delta L \leqslant \Delta L_{max}$，如果 $\Delta L > \Delta L_{max}$，则应在保持合适的焊接速度 v 的前提下适当调整插补周期 T，以调整 ΔL，直至 $\Delta L \leqslant \Delta L_{max}$。假设 $r=30$ mm，$R=50$ mm，$\alpha=60^\circ$，$\varepsilon=0.2$，则根据式(16)可求得 $\Delta L_{max}=6.0$ mm，如果取焊接速度 $v=50$ mm/s，插补周期 $T=25$ ms，则 $\Delta L = v\times T = 1.25\ \text{mm} < \Delta L_{max}$，所选的 v 和 T 满足要求。实际上，根据计算，如果 ΔL 按照 $\Delta L_{max} = v\times T$ 取值，且 v 和 T 均在规定的取值范围内，则插补时只要形成相贯线焊缝的圆柱管半径大于 2 mm，插补结果都能满足给定的逼近误差。表 1 是 $\Delta L_i = 1.25$ mm 时进行插补的计算结果。

表 1　$\Delta L_i = 1.25$ mm 时的插补计算结果

Table 1　Result of interpolation($\Delta L_i = 1.25$)

步数 i	参数增量 $\Delta\varphi_i$ /rad	参数值 φ_i /rad	u 轴增量 ΔU_i /mm	v 轴增量 ΔV_i /mm	w 轴增量 ΔW_i /mm	瞬时角速度 $\omega(t_i)$ /(rad·s^{-1})	实际步长 ΔL_i /mm
1	0.036	0.012π	1.082	−0.608	−0.020	1.443	1.242
2	0.037	0.023π	1.096	−0.581	−0.060	1.463	1.242
3	0.037	0.035π	1.107	−0.552	−0.101	1.483	1.242
4	0.038	0.047π	1.118	−0.522	−0.144	1.503	1.242
5	0.038	0.059π	1.126	−0.490	−0.189	1.522	1.242
6	0.039	0.071π	1.132	−0.457	−0.235	1.541	1.243
7	0.039	0.084π	1.135	−0.422	−0.282	1.559	1.243
…	…	…	…	…	…	…	…
60	0.042	0.783π	−0.953	0.071	−0.806	1.665	1.250
61	0.042	0.797π	−0.985	0.094	−0.765	1.663	1.251
62	0.042	0.890π	−1.015	0.119	−0.722	1.601	1.251
…	…	…	…	…	…	…	…
166	0.035	1.977π	1.052	−0.658	0.058	1.405	1.242
167	0.036	1.988π	1.067	−0.634	0.021	1.423	1.242
168	0.036	1.999π	1.081	−0.609	−0.017	0.036	1.242
169	0.037	2.011π	1.095	−0.583	−0.057	0.037	1.242

从表 1 中可以看出，由式(14)计算出的参数增量 $\Delta\varphi_i$ 是不等长的，而将 $\Delta\varphi_i$ 代入式(7)计算出 ΔL_i 的值的大小基本相等，满足插补要求，可见，插补结果比较稳定。

与焊接件不动只控制焊枪移动的焊接方法(如焊接机器人)相比，作者介绍的自动焊接实时插补控制算法，对于某些焊件的自动焊接实现具有一定的成本优势和方法简单的特点。如 $\alpha=180^\circ$时不论管径大小的两圆管对接，只需简单地控制焊接件的旋转就可以实现自动焊接；而对于小型节点如自行车管架、摩托车管架等焊接件的批量焊接，利用文中介绍的焊接方法简单易行。当然，对于大型节点的焊接，由于节点几何形状大、重量大，需要较大的床体进行装夹，同时还需要功率较大的旋转驱动系统，而对于非批量性生产的焊件的焊接则需要制作、更换各式各样的装夹具，这样利用此方法实现自动焊接则相对困难。对于这些焊接件不宜旋转的情况，文中的控制方法只需要控制焊枪进行三维移动就可以实现复杂相贯线接缝的自动焊接；此时，$\Delta\varphi_i$ 可以不依照公式(14)进行选取，只需要将 φ 从 $0^\circ \sim 360^\circ$ 平均分为 n 等分，即

$$\Delta\varphi = \frac{\varphi}{n}。 \tag{18}$$

这里 n 取自然数，且 n 足够大，以保证 $\Delta\varphi$ 的选取满足误差精度要求。

3　利用 OpenGL 仿真

OpenGL 是一个专业的 3D 程序接口，是一个功能强大、调用方便的 API 形式的底层 3D 图形库。它独立于窗口系统和操作系统，以 OpenGL 为基础开发的应用程序可方便的在各种平台间移植[4]。利用 OpenGL 对焊接插补算法与拟合过程进行仿真。动态仿真过程不仅以非常直观的动画图形在屏幕上再现焊接过程，还可以分析仿真曲线与实际焊缝之间的偏差，进一步对插补算法进行修正、优化。

图 2 为 $r=30$ mm，$R=50$ mm，$\Delta L_i = 1.25$ mm 时焊接运动轨迹的动态仿真截图。

以下动态仿真过程清楚地再现了整个焊接过程中工作台、焊枪的运动轨迹以及焊缝成形位置，从而为数控代码以及所建立的伺服控制算法的校验提供依据。

如果运动控制算法出现错误，则仿真过程就可以清楚地体现出来，如图 3 所示，从而提醒使用人员去检查错误来源，重新调试，直至仿真轨迹完全正确，才能用于实际加工。

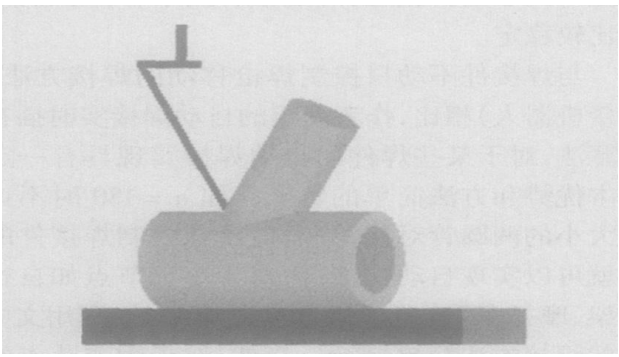

(a) 运动初始状态

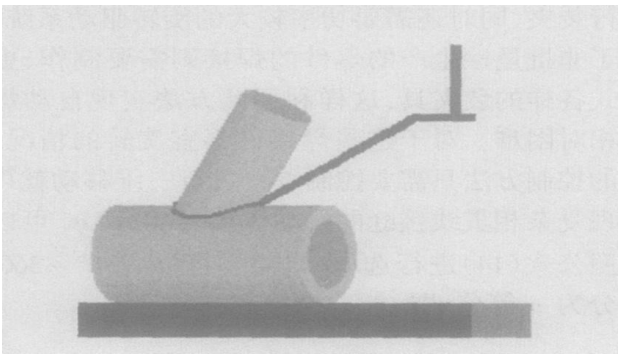

(b) 运动状态

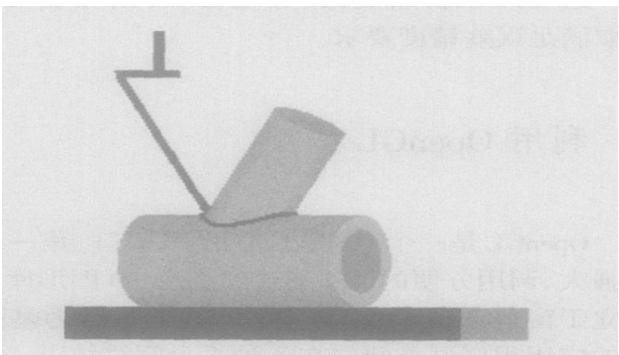

(c) 运动结束状态

图 2 焊接过程动态仿真

Fig. 2 Dynamic simulation of welding process

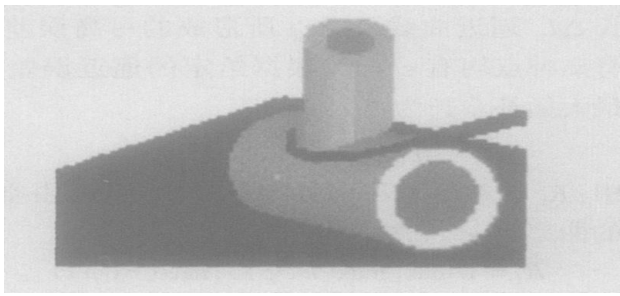

图 3 运动轨迹错误

Fig. 3 Error motion track

4 结 论

(1) 研究的可控步长实时插补控制算法, 可用于实现复杂相贯线接缝自动焊接中的运动算法控制。该算法插补时间固定, 能很好的满足控制系统对实时性的要求, 且插补步长相等, 可以很好的保证轨迹的插补精度。

(2) 利用 OpenGL 工具软件对运动合成轨迹进行了仿真。仿真结果表明, 在满足给定逼近误差的条件下, 通过控制插补步长可得到稳定的插补结果, 为实现质量稳定的焊接过程控制方法奠定了基础。

参考文献:

[1] 金建新. 机床 CNC 系统中任意空间曲线的可控步长插补方法[J]. 机械工程学报, 2000, 36(4): 95-97.

[2] 中国机械工程学会焊接学会. 焊接手册(3)[M]. 北京: 机械工业出版社, 2001.

[3] 林尚扬. 焊接机器人及其应用[M]. 北京: 机械工业出版社, 2000.

[4] 杨武功. OpenGL 三维动画程序设计[M]. 北京: 清华大学出版社, 2000.

作者简介: 霍孟友, 男, 1964 年出生, 工学博士, 副教授。主要研究方向为机电一体化与控制技术, 发表论文 30 余篇。

Email: hmy2618@sdu.edu.cn

and low identification rate. Focused on these problems, the ultrasonic echo characteristics of the spot welding defects were analyzed mainly with the qualitative characteristic parameter analysis, which can identify the spot welding defects quickly through collecting the standard ultrasonic curves and using peak-value marking algorithm. At last, lots of experiments are conducted to prove that this method is credible and efficient for the spot welding of ordinary steel sheets. The identification rate can reach 95%.

Key words: spot welding joints; faulty welding; ultrasonic testing; echo characteristics; fast identification

Design of circuit about new capacitor stored energy spot welding machine ZHOU Hao-bin[1,2], SUN Hui-zhu[1], MA Xiao-mei[1] (1. Xi' an Shiyou University, Xi' an 710065, China; 2. Xi' an Jiaotong University, Xi' an 710049, China). p21—24

Abstract: This paper introduces the design method of a new capacitor stored energy spot welding machine. The new power uses super capacitor to form low voltage capacitor groups instead of high voltage one. The capacitor is charged with direct current chopper circuit, which takes IGBT as the main power machine piece, SKHI22AH4 as the drive circuit, SG3525 as the control chip for PWM, and current feedback in order to get the constant current. In the discharge circuit, the large current is discharged directly through large power SCR without the welding transformer. For the software, 80C552 is the main control chip of the controlling system, so the welding machine could work automatically. The new machine designed has already been used in production and the fine effect was gained to improve the welding quality.

Key words: capacitor stored energy spot welding machine; chopper; super capacitor

Numerical analysis of N_2-Ar protecting tungsten inert gas welding arc LEI Yu-cheng, LI Cai-hui, YU Wen-xia, CHENG Xiao-nong (School of Materials Science and Engineering, Jiangsu University, Zhenjiang 212013, Jiangsu, China). p25—28

Abstract: N_2-Ar protecting tungsten inert gas (TIG) welding arc was chosen as the studied object. A mathematic model was developed according to the theory of magnetic fluid dynamics. TIG welding arc was numerically analyzed based on this 2D, static and axisymmetric model with ANSYS software and the temperature and velocity profiles of the 50%N_2+Ar protecting arc have been simulated. And the difference of the temperature, pressure and velocity of the arc between 50%N_2+Ar protecting arc and Ar protecting arc has been obtained. The results show that the temperature, pressure and velocity of the arc could rise adding N_2 as protesting gas and higher energy density arc can be got.

Key words: tungsten inert-gas welding arc; N_2-Ar protecting; magnetic fluid dynamics; ANSYS

Finite element analysis of residual stresses and thermal deformation for brazing plate-fin structure CHEN Hu, GONG Jian-ming, GENG Lu-yang, TU Shan-dong (College of Mechanical and Power Eegineering, Nanjing University of Technology, Nanjing 210009, China). p29—32, 36

Abstract: This contribution focuses on the analysis of residual stress and thermal deformation of microminiaturized nickel base brazing stainless steel plate-fin structure after vacuum brazing. A finite element method is utilized to conduct the thermal-mechanical analysis for brazing such three layers structure, and the actual heating history of vacuum brazing and temperature-dependent material properties of plate-fin and filler metal are considered. The thermal cycles during brazing, thermal distortion and residual stress after brazing are reported. The results show that plates and fins have different deformation features, and complex stress state appears in the region of joint fillets which may induce the crack generation and propagation of brazed joint and result in the structure failure in service. It is noteworthy to control appropriate brazing time to get preferable joints.

Key words: brazing; plate-fin structure; brazed joint; thermal deformation; residual stresses; finite element method

Analysis on residual stress of hybrid laser-tungste inert gas arc welding of magnesium alloy WANG Hong-yang, CHI Ming-sheng, HUANG Rui-sheng, LIU Li-ming (Materials Modification National Key Laboratory by Laser, Ion and Electron Beams, Dalian University of Technology, Dalian 116024, China). p33—36

Abstract: The residual stress of weld, in both parallel and perpendicular direction, was measured by impacted indentation method for hybrid laser-tungsten inert gas arc welding of magnesium alloy. Based on the date measured, residual stress field simulation was established with finite element method, which can provide a effective supplement to the data of actual measurement. Results showed that the maxium tension stress along the parallel direction of the weld existed at the middle area of the weld was 200-300 MPa, while the maximum compressive stress along perpendicular direction that exists at area of 5 mm and 10 mm to the weld fusion zone was no more than 100 MPa. Through the comparison between actual measurement and simulation, the residual stress distribution characteristics of hybrid laser-tungsten inert gas arc welding of magnesium alloy AZ31B have been well understood.

Key words: residual stress; stress field simulation; impacted indentation method; hybrid welding

Real-time interpolation algorithm and simulation of seam of intersection line for automatic welding HUO Meng-you, WANG Xin-gang, YIN Ping (School of Mechanical Engineering, Shandong Univ., Jinan 250061, China). p37—40

Abstract: Welding of cylinder pipes is one of the common pipe connection, but the line of intersection is a complicated space curve. Based on a special welding machine, it introduces a real-time interpolation algorithm with controllable step length for line of intersection in automatic welding. The concrete method is that using liner

portions with same length to approximate the complicated space curve under the conditions of keeping constant welding speed and satisfying the given approximation error. It takes the general connection form of cylinder pipe for example to illustrate the algorithm, and then OpenGL is used to simulate the composite motion track. Simulation results show that the real-time interpolation algorithm is feasible.

Key words: line of intersection; welding; interpolation algorithm; simulation

Characterization of mechanical properties for aluminium alloy welded joint QIAO Ji-sen, ZHOU Qing-lin, ZHU Liang, CHEN Jian-hong (State Key Laboratory of Gansu Advanced Non-ferrous Metal Materials, Lanzhou University of Technology, Lanzhou 730050, China). p41—44, 49

Abstract: The characterization of local material properties has been evaluated using the punch shearing test. An inversed technique was illustrated to assess the tension behavior of materials from this punch shearing test. In addition, an typical aluminium alloy 6063 and welded joints for auto industry have been tested by the punch shearing procedure to identify the relation between yield strength, ultimate strength and strain-hardening coefficient of local material of welded joint. Results show that the material mechanical properties can be identified accurately by the punch shearing procedure, which will supply the information of joint deformation and failure for aluminium automobile crash assessment.

Key words: punch-shearing test; local mechanical properties; welded joint

Effects of heating time on wettability and spreadability of paste solders on Cu substrate with diode laser soldering system HUANG Xiang, XUE Song-bai, ZHANG Ling, WANG Jian-xin, HAN Zong-jie (College of Materials Science and Technology, Nanjing University of Aeronautics and Astronautics, Nanjing 210016, China). p45—49

Abstract: Diode laser soldering system was used to study and explore the ways to improve the wettability and spreadability of Sn63Pb37 paste solder and Sn96Ag3.5Cu0.5 lead-free paste solder on Cu substrate. The effects of heating time of the laser on the wettability of paste solders were investigated and it was also analyzed that the microstructures of the joints and interfacial region of Sn63Pb37 and Sn96Ag3.5Cu0.5 under different time conditions by means of SEM. The Results indicate that the wettability and spreadability of the two kinds of solders on Cu substrate are improved with the increase of heating time under the condition of selected laser output power. When the heating time is longer than 1.5 s, the spreading area and wetting angle of Sn63Pb37 solder are tending towards stability and when the heating time is longer than 2.5 s, the spreading area and wetting angle of Sn-Ag-Cu solder are tending towards stability as well.

Key words: diode laser soldering; wettability; Sn-Pb solder; Sn-Ag-Cu solder

Friction welding technology between titanium alloy and pure aluminum BAI Jian-hong, FU Li, DU Sui-geng (College of Materials Science, Northwestern Polytechnical University, Xi'an 710072, China). p50—52

Abstract: Titanium alloy and aluminum alloy are good for the structure materials in the fields of aerospace and aviation because of their excellent properties. It is necessary to join these two materials for wider applications. TC4 titanium alloy and L5 pure aluminum are joined by friction welded and then post-welding tempering treatment have been conducted. By means of the optical microscope detecting, EDX analysis, micro-sclerometer and tensile test, we explore experimentally the microstructure characteristics and diffusion behavior of the friction welded joint of TC4 titanium alloy and L5 pure aluminum. As expected, there are good friction weldability between TC4 titanium alloy and L5 pure aluminum and no intermetallic phases created in friction welding zone under the welding parameters used in this trial. Furthermore, the tensile strength of the welded joint exceeds that of the base metal aluminum. After post-welding heat treatment, the diffusion zone of main alloying elements Ti, Al and V widens and the microhardness of the friction welded joints near titanium increases greatly because of the aging effect.

Key words: friction welding; post-welding heat treatment; TC4 titanium alloy; L5 pure aluminum; microstructure

MAG welding molten pool image character and useful information analysis WANG Ke-hong, SHEN Ying-ji, QIAN Feng, YOU Qiu-rong (Dept of materials, Nanjing University Science & Technology, Nanjing 210094, China). p53—56

Abstract: A passive vision sensing system for taking the image of MAG welding molten pool has been set up. Near-infrared CCD and compound filters system composed of 1 064 nm narrow-band filer and 0.1% neutral dimmer film are used to eliminate the arc light disturbance and a lot of clear images are obtained. Image-processing software is used to extract the characteristic information which reflects the welding quality. For the single image, the gray character is analyzed and three equivalent contour lines are obtained. For continuous multi-frame images, the image aberration shade detection and mean gray distribution are put forward to study the process of MAG welding.

Key words: metal active-gas welding; molten pool image; characteristic information; gray analysis

Numerical simulation of hydrogen diffusion under welding residual stress JIANG Wen-chun, GONG Jian-ming, TANG Jian-qun, CHEN Hu, TU Shan-dong (College of Mechanical and Power Engineering, Nanjing University of Technology, Nanjing 210009, China). p57—60, 64

Abstract: Using finite element analysis code ABAQUS, a sequential coupling calculating program on hydrogen diffusion has been developed. Using this program, the effect of as-welded residual stress on the hydrogen diffusion was numerically simulated for the